Joint data rate and EMF exposure analysis in Manhattan environments: stochastic geometry and ray tracing approaches

Charles Wiame, *Member, IEEE*, Simon Demey, *Member, IEEE*, Luc Vandendorpe, *Fellow, IEEE*, Philippe De Doncker, *Member, IEEE*, and Claude Oestges, *Fellow, IEEE*

Abstract—The objective of this study is to jointly analyze the data rate and electromagnetic field (EMF) exposure in urban environments. Capitalizing on stochastic geometry (SG), a network level analysis is performed by modelling these environments via Manhattan Poisson line processes (MPLP). Using this framework, a number of performance metrics are derived: first moments, marginal distributions and joint distributions of the data rate and exposure. In addition, the original Manhattan model is generalized to include advanced features: corner diffraction, presence of potential blockages in streets, and users positioned at crossroads. As a second approach, deterministic ray tracing (RT) is utilized to compute the same metrics. The two methods are shown to provide close results on the condition that the model parameters are coherently selected. Furthermore, the numerical results enable to gain insight into several aspects: the role of the propagation mechanisms in the performance metrics, existing trade-offs between the rate and exposure requirements, as well as the impact of the user location (at a crossroad or in a single street).

Index Terms—EMF exposure, stochastic geometry, ray tracing, Manhattan Poisson line process.

I. INTRODUCTION

From Bell Labs perspective, the global data traffic is expected to skyrocket in future wireless networks [1]. The increasing number of mobile devices and the growing usage of data-consuming applications are two of the main factors supporting this prediction [2]. In order to satisfy the resulting increase in capacity demand, [3] identifies the densification of base stations (BS) as a promising solution. One possible manner to implement this densification consists in deploying small cell BSs to offload macro BSs. This approach is shown to achieve better spectral efficiency and to extend coverage regions [4]. According to the study in [5], it is expected to find up to 40-50 BSs/km² to meet the coverage requirements expected for 5G and beyond. However, such intensive densification may raise questions in terms of sustainability, cost, and human exposure (for which legal thresholds must be respected in some countries). The analysis of this study focuses on this last exposure aspect.

The first areas where the densification is likely to be planned are city centers, which feature a particularly high user activity.

Compared to other environments (suburbs or rural areas), these sites are also characterized by an important density of blockages impacting the propagations conditions. Channels models characterizing these environments should hence include this blockage aspect with accuracy. A number of techniques have been investigated to this purpose: ray-tracing (RT) [6], Winner-type models [7], COST-type models [8], etc. Each of these approaches has its own specificities and is more or less suitable for a network-level analysis. On the one hand, some of the deterministic tools (e.g. ray tracing) have the advantage of modelling the physical propagation with accuracy, but they often require important computational resources [9]. On the other hand, BS densification is likely to induce additional randomness in future networks: in the user activity, node positions, etc. This justifies the use of stochastic models, which may be of interest at a large network scale. From a global network perspective, some of the link-level details are often abstracted or simplified when using such methods. This enables to meet computational constraints, but comes at the cost of simplifications in the propagation mechanisms. Stochastic geometry (SG) is one of the tools enabling to study the global performance at such network level [10]. This branch of spatial statistics abstracts base stations and users as random point processes. On the basis of these processes, analytical expressions of metrics can be derived: coverage probability, spectral efficiency, etc. These expressions are averaged out over all the potential node locations, and therefore capture the full spatial statistics. Such an approach therefore enables to circumvent brute force Monte Carlo (MC) simulations. Within the SG theory, two point processes are employed to model urban topologies: the Manhattan Poisson line process [11] (MPLP, used to represent streets with a regular grid structure), and the Cox process [12] (use to represent cities with irregular street deployments). This work considers the former topology, and attempts to compare results obtained via RT and SG for this urban environment.

A. Related works

The study in [11] is one of the first SG works employing the MPLP to model roads. The coverage distribution is derived using a correlated blockage model accounting for building penetration. In [13], the same metric is analyzed for vehicle-to-infrastructure networks operating at mmWave frequencies. The MPLP is shown to accurately describe

Manhattan networks by comparison with the fixed grid model and the actual street deployment in Chicago. MPLP models are also used for indoor scenarios [14–16], drones-to-ground networks [17] and relay assisted networks [18]. Other works also consider Cox line processes as generalization of the MPLP to model non-prependicular streets [12, 19–25]. Among the different technologies that have been studied, one can mention vehicle-to-everything communication [19], vehicular ad hoc networks [23] and multi-radio access technology [25]. In [19], trends on the network deployment design have been highlighted and the benefit of small cells to offload macro BSs has been proven.

Many works focus on the analysis of emerging networks using pure SG approaches. However, a very limited number of publications propose validations of these SG models using other methods (comparison to datasets, measurements, or softwares capturing additional electromagnetic phenomenons such as diffraction or scattering, etc). In [26], an experimental validation is conducted using two open access databases of mobile operators in United Kingdom. More recently, [27] validated a radar detection analysis of using finite difference time domain technique. To the best of the authors knowledge, no validation of SG models using other software tools (e.g. RT) can be found in the literature.

B. Contributions

On the basis of the aforementioned works, the main findings of this study can be summarized as follows:

- The Manhattan model originally presented in [11] is fully revisited. A number of features are added to this model to capture additional propagation aspects. These new characteristics are detailed below:
  - The proposed analysis takes into account power contributions coming from BSs outside the user street and propagating via diffraction at crossroad corners. As explained in [13], contributions from such a corner diffraction can be significant compared to building penetration, hence the need to address their modelling. To this purpose, Berg recursive method is employed for its simplicity and its accuracy regarding the path loss (PL) levels [28]. This model also has the advantage of featuring a general expression, depending on both Euclidean distances and corner angles. These dependencies open perspectives for a generalization to Cox processes, and differ from [13] where constant diffraction losses are considered.
  - Unlike [11] where the small scale fading was only Rayleigh, our framework enables to incorporate any fading distribution in the model.
  - The presence of street obstacles (cars, trucks,...) is included using the blockage model of [29], and integrated in the SG framework via inhomogeneous thinning. This thinning is function of a line-of-sight (LOS) probability which is distance dependent and continuous everywhere, unlike the LOS ball model [30].

  - In practical deployments, a non-negligible proportion of users can be located at street intersections (e.g. pedestrians waiting at traffic lights). In such cases, the simultaneous presence of BSs in the two crossing streets results in power levels differing from those measured at other users. In the original work of [11], users were almost surely never located at street intersections. Conversely, our work includes a non-zero probability for this event to happen, in which case power signals coming from the two perpendicular streets are considered.
  - The heights of the UEs and BSs are here considered. Neglecting this feature might result in underestimations in the PLs, especially for BSs in the user vincinity. The power contributions associated to these BSs might hence be overestimated, which could bias the performance metrics.
- To the best authors' knowledge, this analysis is the first work studying EMF exposure in Poisson line processes. In order to characterize the statistics of exposure and its correlation to the spectral efficiency, the following metrics are derived: the first moments of the data rate and exposure, their marginal distributions, as well as their joint distribution.
- Most SG publications validate their analytical results using equivalent MC simulations. While such procedure enables to verify the correctness of the derived expressions, it does not provide indications on whether or not they are realistic compared to more physical propagation models. This study attempts to bridge the resulting gap by comparing our SG expressions to RT simulations reproducing the Manhattan environment. To our best knowledge, this paper is the first work performing such RT validation. From this comparison, we conclude that the two approaches can produce tight results. Selecting the propagation parameters of the SG framework appropriately is however a necessary condition to obtain an accurate matching. A method is proposed in section V to properly tune these parameters. A sensitivity analysis is also performed in the same section to support these conclusions.

C. Organization of the paper

The system model and the analyzed metrics are defined in Section II. The SG expressions of these metrics are derived in Section III. The numerical results of the SG analysis are presented in Section IV. A case study comparing the SG and RT frameworks is then detailed in section V. Section VI finally summarizes the takeaways of this study, and provides future research directions.

Notations: in the next sections, $j = \sqrt{-1}$ denotes the imaginary unit. $\mathrm{Im}\{\cdot\}$ represents the imaginary part of a complex number. $\mathbf{x}^H$ is the conjugate transpose of matrix $\mathbf{x}$.

II. SYSTEM MODEL

A. Network topology

One considers a street infrastructure deployed in a square area of length $2R$ and centered around $(0,0) \in \mathbb{R}^2$. This

deployment is modelled by means of a MPLP: horizontal and vertical streets are built using two independent Poisson point processes (PPP) denoted by Φ_{VS} and Φ_{HS}. The density of these PPPs is here constant and given by λ_S. The empty spaces between these streets are assumed to be buildings.

Base stations are generated in each street using independent PPPs of density λ_B. In the following sections, the total set containing all these BSs will be denoted as Φ_B. These BSs operate at frequency f and are placed at height H_B. In addition, they are all equipped with a single antenna of unit gain. One will denote as P_B their constant and isotropic transmit power.

The network analysis is performed for a typical UE located at $(0, 0, H_U)$. One will denote $\Delta H = H_B - H_U$, its height difference with respect to the BSs. In the framework of this work, this difference is assumed to be greater than 1 meter to avoid path loss singularities (see Subsection II-D). The UE is also equipped with a single isotropic antenna of unit gain. As discussed in the previous section, the location of this UE will strongly impact the received power levels: users located at crossroads are in average more exposed to LOS signal compared to users that are not located at street intersections. To take this feature into account, the analysis proposed in this study is performed in two steps:

1) Street and crossroad UEs are first separately investigated. The performance metrics are independently derived for each of these two user types. In the case of the crossroad UE, two streets (of ordinate $y = 0$ and abscissa $x = 0$) are added to the MPLP to model the intersection (see Figure 1). By contrast, a single avenue (of ordinate $y = 0$) is generated for the street UE (Figure 1). These additional lines in which the typical user is located will be referred to as *typical streets* in the rest of this document.

2) General metrics are deduced for an arbitrary UE possibly located at a crossroad with probability[1] η and in a street with probability $1 - \eta$. The expressions for these final metrics are derived using a weighted average depending on this parameter η.

B. Association policy

For sake of mathematical tractability, the typical user is associated to the closest BS of its typical street(s). The selected BS is hence the candidate in this typical street(s) minimizing the 1D distance to the user. The other BSs of Φ_B are assumed to provide interference. Under this policy, the distribution of the distance from a street user to its serving BS is known and provided in [31].

$$f_{r,1}(r) = \frac{2\lambda_B e^{-2\lambda_B r}}{1 - e^{-2\lambda_B R}}, \quad \text{for } 0 < r < R. \tag{1}$$

For users located at crossroad, the distribution considers the presence of the two streets:

$$f_{r,2}(r) = \frac{4\lambda_B e^{-4\lambda_B r}}{1 - e^{-4\lambda_B R}}, \quad \text{for } 0 < r < R. \tag{2}$$

[1]This probability η can for instance be defined as the ratio between the streets and building widths.
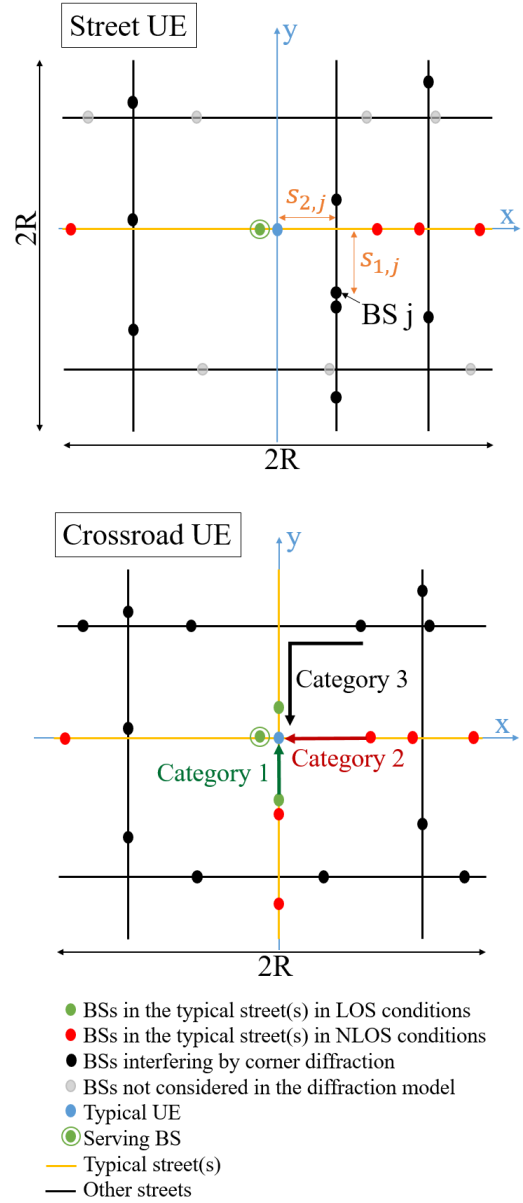

Fig. 1: Illustration of the topology in the cases of a street user and of a crossroad user.

Remark 1: A generalization to a strongest average power association is possible and left for future work. In the framework of this study, it is possible to show that the two rules lead to similar results for low blockage probabilities.

C. Blockage model

Obstacles (vehicles, urban furniture, etc) are assumed to be present in the typical street(s). These blockages are assumed to induce non line-of-sight (NLOS) links for some of the BSs. In order to model this aspect, the probabilities used in [29] are employed: given a BS in the typical street(s) located at distance r from the user, the probability for this BS to be in LOS is given by $p_L(r) = e^{-\beta r^\gamma}$, with $\beta, \gamma \in \mathbb{R}^+$. In a complementary way, the probability of NLOS is given by $p_N(r) = 1 - p_L(r)$.

D. Computation of the received powers

The analysis of this study distinguishes three categories of received power signals. These categories are detailed hereafter and represented in Figure 1.

Category 1 - LOS BSs in the typical street(s): the power received at the typical UE i^* from a LOS BS j of the typical street(s) is given by

$$P_{i^*j}^{(SG)} = P_B \left| h_{i^*j}^{(L)} \right|^2 \kappa_L^{-1} \sqrt{d_{i^*j}^2 + \Delta H^2}^{-\alpha_L}. \quad (3)$$

In this definition, $\left| h_{i^*j}^{(L)} \right|^2$ accounts for the small scale fading. κ_L and α_L respectively represent the intercept and path loss exponent of the path loss model. d_{i^*j} denotes one-dimensional distance from UE i^* and BS j.

Category 2 - NLOS BSs in the typical street(s): the expression of the powers received from these BSs is similar to category 1:

$$P_{i^*j}^{(SG)} = P_B \left| h_{i^*j}^{(N)} \right|^2 \kappa_N^{-1} \sqrt{d_{i^*j}^2 + \Delta H^2}^{-\alpha_N} \quad (4)$$

The difference with the LOS category is related to the PL parameters κ_N and α_N, and the fading coefficients $\left| h_{i^*j}^{(N)} \right|^2$. These variables can take values/distributions different from κ_L, α_L and $\left| h_{i^*j}^{(L)} \right|$, enabling more severe attenuations on the NLOS links.

Category 3 - Corner diffraction: the power contributions of this third category are associated to BSs located in avenues perpendicular to the typical street(s) (Fig. 1). These powers affect the typical UE via corner diffraction and are modelled using Berg recursive method [28]. The power received from BS j is in that case given by:

$$P_{i^*j}^{(SG)} = P_B \left| h_{i^*j}^{(D)} \right|^2 \kappa_D^{-1} \mathcal{D}_b(s_{1,j}, s_{2,j})^{-\alpha_D} \quad (5)$$

where κ_D, α_D and $\left| h_{i^*j}^{(D)} \right|^2$ are respectively the PL and the fading power coefficients associated to this category of signals. The variable $\mathcal{D}_b(s_{1,j}, s_{2,j})$ represents the Berg distance. For a unique building edge diffraction, it is defined as

$$\mathcal{D}_b(s_{1,j}, s_{2,j}) = s_{1,j} + s_{2,j} + k_f \left(\frac{\theta_{i,j}}{\pi/2} \right)^\nu s_{1,j} s_{2,j}. \quad (6)$$

In this definition, $k_f = \sqrt{\frac{q_\lambda f}{c}}$ where q_λ is a frequency dependent model parameter and c is the speed of light. If the system is operated at a frequency between 2 and 6 GHz, q_λ can be fixed at 0.031 for urban micro-cells [32]. $\theta_{i,j}$ is the angle between the street of BS j and the street of user i^*. Its value is always equal to $\pi/2$ in the case of the MPLP. ν is an empirical parameter which has no influence in this study. Finally, the variables $s_{1,j}$ and $s_{2,j}$ denote the distances from BS j to the street corner and from the street corner to user i^* (cfr Figure 1).

Remark 2: one will note that $\mathcal{D}_b(\cdot, \cdot)$ is greater than the Euclidean distance from i^* to j, owing to the diffraction loss.

Remark 3: contributions associated to building penetration are here neglected. As mentioned in [13], this assumption is particularly true for mmWaves. For scenarios where this

hypothesis may not be valid, the inclusion of these contributions as fourth category is left for future works. In addition, equations (5) and (6) constitute the first order Berg model: signals diffracted more than once are not considered here.

Remark 4: an exclusion zone is considered in the street generation to prevent the path loss in (5) to be greater than 1. This zone is defined as a segment $[-r_s; r_s]$ around the typical user. Streets potentially generated in this zone are ignored. Regarding the other path loss models of (3) and (4), potential singularities are circumvented thanks to parameter $\Delta H > 1$.

Remark 5: in this mathematical framework, all the fading coefficients can take any distribution of known characteristic function. In the numerical results presented in section IV, one will however focus on the particular case of Rice fading for categories 1 and 2, and Rayleigh fading for category 3.

E. Performance metrics

The metrics studied in this work are detailed below.

- The average user capacity is defined as

$$\mu_C = \mathbb{E}\Big[B \log_2 \left(1 + \text{SINR}_{i^*}\right) \Big] \quad \text{where} \quad (7)$$

$$\text{SINR}_{i^*} = \frac{P_{i^*j^*}}{\sum\limits_{\substack{j \in \Phi_B \\ j \neq j^*}} P_{i^*j} + W} = \frac{S}{I_L + I_N + I_D + W}. \quad (8)$$

In the above expressions, B is the system bandwidth. P_{ij} represents the power transmitted from BS i to UE j. j^* is the index of the serving BS. The variables S, I_L and I_N represent the useful signal power and the interference associated to LOS and NLOS BSs of the typical street(s). I_D denotes the interference associated to corner diffraction. W finally represents the constant noise power.

- The average exposure coming from all network BSs is defined as

$$\mu_E = \mathbb{E}\Bigg[\sum_{j \in \Phi_B} P_{i^*j} \Bigg] = \mu_L + \mu_N + \mu_D, \quad (9)$$

where μ_L, μ_N and μ_D are respectively the mean total powers coming from the typical street(s) in LOS condition, from the typical street(s) in NLOS condition, and associated to diffraction. With a slight abuse of notation, S is here included either in μ_L or in μ_N.

- The coverage probability is defined as

$$P_c(\theta_c) = \mathbb{P}\big[\text{SINR}_{i^*} > \theta_c \big]. \quad (10)$$

Remark 6: the distribution of the capacity is defined as $P_{cap}(\theta) = \mathbb{P}\big[B \log_2 \left(1 + \text{SINR}_{i^*}\right) > \theta \big]$ and can directly be deduced via the change of variable $P_{cap}(\theta) = P_c(2^{\frac{\theta}{B}} - 1)$.

- the cumulative distribution function (CDF) of the exposure is defined as

$$P_e(\theta_e) = \mathbb{P}\Bigg[\sum_{j \in \Phi_B} P_{i^*j} < \theta_e \Bigg] \quad (11)$$

where $\sum_{j \in \Phi_B} P_{i^*j} = S + I_L + I_N + I_D. \quad (12)$

- The joint SIR-exposure distribution is defined as

$$F(\theta_c, \theta_e) = \mathbb{P}\left[\text{SINR}_{i^*} > \theta_c, \sum_{j \in \Phi_B} P_{i^*j} < \theta_e\right]. \quad (13)$$

This distribution represents the probability for a mobile user to satisfy coverage requirements (SINR greater than θ_c) while experiencing an exposure below a safety threshold θ_e.

Remark 7: this metric differs from the joint distribution of [33], where the exposure is required to be above a threshold for energy harvesting purposes. To the best of the authors knowledge, no work in the literature has considered (13) at the moment of writing this study.

III. ANALYTICAL RESULTS

In this section, the index $q = \{1,2\}$ is used to denote expressions related to a street UE and to a crossroad UE respectively.

A. Preliminaries: characteristic functions

A few characteristic functions (CF) are first introduced since they will be necessary to compute the performance metrics. All these CFs are conditioned on $r = d_{i^*j^*}$, the distance between the typical UE and its serving BS.

1) Fading models:

All results of this section are developed to be applicable for any fading distribution. For this reason, they are systematically expressed as functions of the general CF of the fading model, denoted by $\phi_F(\cdot)$. The distributions that are selected as particular cases to generate the numerical results of section IV are provided below:

– Rice fading is chosen for BSs in the user street(s). The CF of this fading model is given by Lemma 4.6 in [34]:

$$\phi_F(t; K) = \frac{K+1}{K+1-jt} \exp\left[\frac{Kjt}{K+1-jt}\right] \quad (14)$$

where K is the K-factor of the distribution.
– Rayleigh fading is considered for BSs interfering via diffraction. The associated CF can be expressed as $\phi_F(t; K = 0)$.

2) CF of the useful received power:

The CF of the useful received power is given by

$$\phi_S^{(p)}(t|r) = \phi_F\left(P_B\kappa_p^{-1}\sqrt{r^2 + \Delta H^2}^{-\alpha_p} t; K\right) \quad (15)$$

where $p = \{L, N\}$ depending on whether the serving BS is in LOS or NLOS conditions.
Proof 1: the result comes from the definition of the useful power, given by (3) or (4).

3) CFs of the interference affecting street users:

- The CF of the LOS interference coming from the typical street is given by equation (16) next page.
  Proof 2: The proof is available in Appendix A.
- The CF of the NLOS interference coming from the typical street is given by equation (17).
  Proof 3: The proof follows the same approach as the proof of equation (16).
- The CF of the interference associated to first order diffraction is given by equation (18).
  Proof 4: The proof is available in Appendix B.

4) CFs of the interference affecting crossroad users:

The expressions derived for the street UE can be easily generalized to the crossroad UE. Taking into account the double presence of access points, the following expressions are obtained:

$$\phi_{L,2}(t|r) = \phi_{L,1}^2(t|r)$$
$$\phi_{N,2}(t|r) = \phi_{N,1}^2(t|r) \qquad \phi_{D,2}(t) = \phi_{D,1}^2(t|r). \quad (19)$$

B. Coverage probability

The coverage probability is given by equation (20) where $q = 1$ for a street UE and $q = 2$ for a crossroad UE.
Proof 5: The proof is available in Appendix C.

C. Exposure distribution

The CDF of the exposure can be expressed as equation (21).
Proof 6: The developments follow the same reasoning as Appendix C.

D. Joint SIR-exposure distribution

A lower bound (LB) for the joint SIR-exposure distribution can be expressed as:

$$\bar{F}_q(\theta_c, \theta_e) = \max\left(0, P_{c,q}(\theta_c) + P_{e,q}(\theta_e) - 1\right). \quad (22)$$

Proof 7: This result comes from the application of Fréchet inequalities [35].

E. Average capacity

The average user capacity is given by equation (23) where $g(t) = t^{-1}e^{-tW}$.
Proof 8: The proof consists in applying the lemma proposed in equation (2) of [36]. The other steps follows the same reasoning as Appendix C.

F. Average exposure

The average exposure received at a street UE can be decomposed as

$$\mu_{E,1} = \mu_{L,1} + \mu_{N,1} + \mu_{D,1} \quad (24)$$

$$\phi_{L,1}(t|r) = \exp\left[2\lambda_B \int_r^R p_L(r')\left[\phi_F\left(P_B\kappa_L^{-1}\sqrt{r'^2 + \Delta H^2}^{-\alpha_L}t; K\right) - 1\right]dr'\right] \tag{16}$$

$$\phi_{N,1}(t|r) = \exp\left[2\lambda_B \int_r^R p_N(r')\left[\phi_F\left(P_B\kappa_N^{-1}\sqrt{r'^2 + \Delta H^2}^{-\alpha_N}t; K\right) - 1\right]dr'\right] \tag{17}$$

$$\phi_{D,1}(t) = \exp\left[-2\lambda_S \int_{r_s}^R 1 - \exp\left[-2\lambda_B \int_0^R 1 - \phi_F\left(P_B\kappa_D^{-1}\mathcal{D}_b(x,y)^{-\alpha_D}t; 0\right)dx\right]dy\right] \tag{18}$$

$$P_{c,q}(\theta_c) = \frac{1}{2} + \frac{1}{\pi}\int_0^\infty Im\left[\phi_{D,q}(-\theta_c t)\int_0^R p_L(r)\phi_S^{(L)}(t|r)\phi_{L,q}(-\theta_c t|r)\phi_{N,q}(-\theta_c t|r)f_{r,q}(r)dr\right]t^{-1}dt$$
$$+ \frac{1}{\pi}\int_0^\infty Im\left[\phi_{D,q}(-\theta_c t)\int_0^R p_N(r)\phi_S^{(N)}(t|r)\phi_{L,q}(-\theta_c t|r)\phi_{N,q}(-\theta_c t|r)f_{r,q}(r)dr\right]t^{-1}dt \tag{20}$$

$$P_{e,q}(\theta_e) = \frac{1}{2} - \frac{1}{\pi}\int_0^\infty Im\left[e^{-jt\theta_e}\phi_{D,q}(t)\int_0^R p_L(r)\phi_S^{(L)}(t|r)\phi_{L,q}(t|r)\phi_{N,q}(t|r)f_{r,q}(r)dr\right]t^{-1}dt$$
$$- \frac{1}{\pi}\int_0^\infty Im\left[e^{-jt\theta_e}\phi_{D,q}(t)\int_0^R p_N(r)\phi_S^{(N)}(t|r)\phi_{L,q}(t|r)\phi_{N,q}(t|r)f_{r,q}(r)dr\right]t^{-1}dt \tag{21}$$

$$\mu_{C,q} = \frac{B}{\ln(2)}\left[\int_0^\infty g(t)\phi_{D,q}(jt)\int_0^R p_L(r)\left(1 - \phi_S^{(L)}(jt|r)\right)\phi_{L,q}(jt|r)\phi_{N,q}(jt|r)f_{r,q}(r)drdt\right.$$
$$\left.+ \int_0^\infty g(t)\phi_{D,q}(jt)\int_0^R p_N(r)\left(1 - \phi_S^{(N)}(jt|r)\right)\phi_{L,q}(jt|r)\phi_{N,q}(jt|r)f_{r,q}(r)drdt\right] \tag{23}$$

where the average exposures associated to the three categories of powers are given by

$$\mu_{L,1} = \int_0^R P_B\kappa_L^{-1}2\lambda_B p_L(r)\sqrt{r^2 + \Delta H^2}^{-\alpha_L}dr \tag{25}$$

$$\mu_{N,1} = \int_0^R P_B\kappa_N^{-1}2\lambda_B p_N(r)\sqrt{r^2 + \Delta H^2}^{-\alpha_N}dr \tag{26}$$

$$\mu_{D,1} = \int_0^R \int_{r_s}^R P_B\kappa_D^{-1}\left[r + r' + qrr'\right]^{-\alpha_D}4\lambda_S\lambda_B drdr'. \tag{27}$$

Proof 9: The proof follows from the application of Campbell theorem [37].

The average exposure of a crossroad UE is then easily deduced: $\mu_{E,2} = 2\mu_{E,1}$.

G. Generalization to an arbitrary UE

All the above metrics can be generalized to the case of an arbitrary UE (possibly located in a crossroad or a single street with probabilities η and $1 - \eta$). Using the law of total probability, one has for each metric:

$$m = (1 - \eta)m_1 + \eta m_2 \tag{28}$$

where m is the considered metric, m_1 is its expression for the street UE and m_2 its expression for the crossroad UE. The general variables $P_c(\theta_c)$, $P_e(\theta_e)$, $\bar{F}(\theta_c, \theta_e)$, μ_E and μ_C can hence be obtained in this manner.

IV. NUMERICAL RESULTS OBTAINED VIA STOCHASTIC GEOMETRY

In order to generate the results of this section, a network of infinite size is considered: the network size R is hence set to $+\infty$ in the analytical expressions, and to $128km$ in the MC simulations (value sufficiently large to reproduce an infinite environment from the point of view of the centric user).

A. Impact of the propagation mechanisms

In this section, the roles of blockages and of diffraction are successively investigated. In order to study the impact of blockages, Figure 2 displays the coverage and the exposure evaluated for different LOS probabilities. For the studied cases, different values of the parameter β (defining the LOS probability) are considered while the parameter γ is fixed. The analytical results are validated using MC simulations and compared to the case without blockages ($\beta = 0$). The evolution of the exposure (Figure 2b) is trivially explained by the presence of NLOS links, which increases with β and reduces the received power. Regarding the coverage (Figure 2a), two opposite scenarios can arise when introducing obstacles:

- Scenario 1: the serving BS is in LOS and some of the interferers are in NLOS; this enhances the coverage probability when comparing to a case with no obstacle in the network.
- Scenario 2: the serving BS is NLOS while some interferers are still in LOS; this deteriorates the coverage probability.
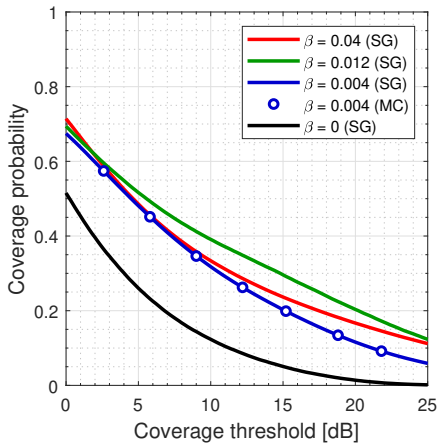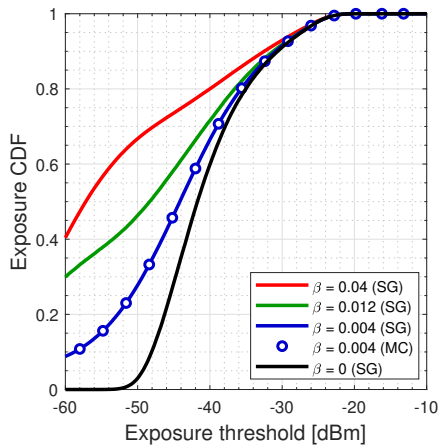
(a) Coverage probability $P_c\left(\theta_c\right)$ for an arbitrary UE.

(b) Exposure CDF $P_e\left(\theta_e\right)$ for an arbitrary UE.

Fig. 2: Analysis of the impact of β. The parameters selected are $h_U = 1.5m$, $h_B = 6m$, $\lambda_S = 5/km$, $\lambda_B = 5/km$, $P_B = 1W$, $f = 3.6GHz$, $\alpha_L = 1.7$, $\alpha_N = 2.5$, $\alpha_D = 3.5$, $\eta = 0.1$, $\gamma = 1$ and $K = 6$.

These scenarios explain the impact of obstacles on the coverage. When progressively increasing the blockage probability up to $\beta = 0.012$, improvements in the coverage can be observed. These improvements therefore correspond to realizations associated to above scenario 1. By contrast, further increasing β to 0.04 reduces the coverage. This decrease is in turn explained by a higher number of realizations corresponding to scenario 2 (due to the high value of β), which is detrimental to the coverage.

The graphs of Figure 3 quantify the influence of diffraction on the performance. For each of these graphs, coverage probabilities are shown for coverage thresholds of 0, 5, 10 and 15 dB. The continuous and dashed lines respectively represent the values obtained with and without diffracted signals taken into account. Figure 3a illustrates the evolution of these probabilities as function of the street density. Furthermore, it is also possible to show that the relative impact of diffraction can be more significant in street realizations characterized by a locally low BS density. For such cases, incident powers coming from BSs located outside the user street itself can proportionally have larger impacts on the coverage. Figure 3b illustrates this statement by fixing the BS density λ_B^t in the user street and by progressively increasing the BS density in the other streets, denoted by λ_B^d in the legend. For a $5dB$ threshold, the inclusion of diffracted signals results in a decrease in coverage of around 0.06 if the BS density is identical in all streets ($\lambda_B^d/\lambda_B^t = 1$). When increasing the BS density in adjacent streets, this gap increases to 1.4 for $\lambda_B^d/\lambda_B^t = 4$.

B. Joint coverage and exposure distribution

Figure 4 illustrates the joint coverage and exposure distribution. The SG lower bound of (22) is represented as function of the two thresholds θ_c and θ_e in Figure 4(a). This bound is then compared to the MC simulations in Figure 4(b) for fixed values of θ_c. One can observe on this graph that the probability of obtaining a low exposure decreases as the coverage threshold increases. This observation is due to the useful received power S, present in both SINR and exposure definitions. This power will statistically be high for users in good coverage, which increases for these users the probability to experience a high exposure. Some trade-offs are therefore necessary in the coverage and exposure requirements.

C. User type comparison

Figure 5 compares the performance achievable for a street (st.) UE and for a crossroad (cr.) UE. Figure 5a shows the average user capacity as a function of the BS density. Independently of the UE type, one can note the existence of an optimal value for this quantity, as already shown in previous works [38]. For a low BS density, the signal-to-noise ratio takes low values, to the detriment of the capacity. As the BS density progressively increases, the serving BS statistically becomes closer to the UE, which increases the useful received power. The densification hence enables to increase the average capacity, up to some optimum $\lambda_B = \lambda_B^{opt}$. Beyond this maximum, the improvements in useful power no longer compensate the increase of interference, resulting in a decreasing capacity. One will note that the optimal capacity associated to street users is reached for a higher BS density compared to the optimal capacity of crossroad users. This difference is due to the presence of BSs which is in average doubled for crossroad users (due to the two streets forming the intersection). In Figure 5b, isocurves of the joint SIR-exposure metric are analysed. Each curve represents the set of thresholds (θ_c, θ_e) satisfied with probability $p \in \{0.1, 0.5, 0.85\}$, for a street or a crossroad user. One can here observe that the achievable performance of the street user is higher than the crossroad user. One justification of this difference comes from the exposure of the crossroad user, which is in average doubled compared to the street user. At a given coverage requirement, the probability for the crossroad user to satisfy an exposure threshold is therefore reduced compared to the street user.
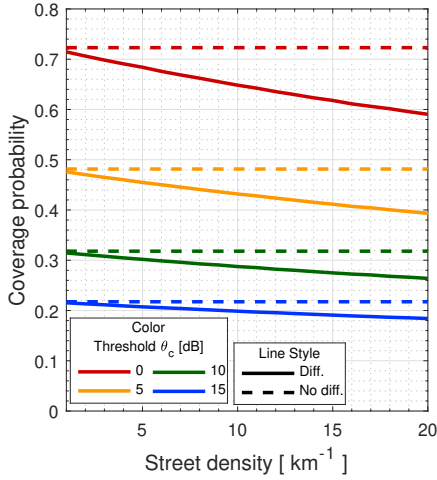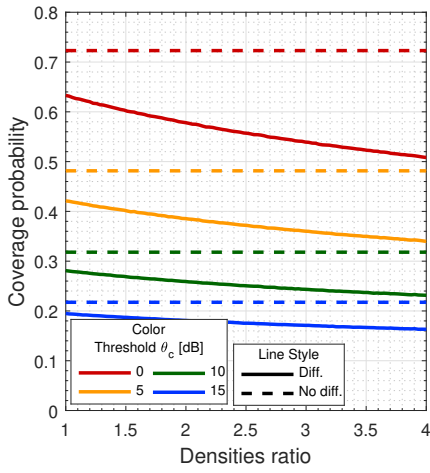
(a) Impact of λ_S on $P_{c,1}$.

(a) Lower bound on joint metric $F(\theta_c, \theta_e)$ for an arbitrary UE.

(b) Impact of $\lambda_B^d / \lambda_B^t$ on $P_{c,1}$.

Fig. 3: Impact of the BS and street densities. Unless stated otherwise, the selected parameters are $h_U = 1.5m$, $h_B = 6m$, $\lambda_S = 12.5km^{-1}$, $\lambda_B = 3km^{-1}$, $P_B = 1W$, $f = 2GHz$, $\alpha_L = 1.7$, $\alpha_N = 2.5$, $\alpha_D = 2.5$, $\kappa_L = \kappa_N = \kappa_D = (4\pi f/c)^2$, $\beta = 0.04$, $\gamma = 1$ and $K = 6$.

(b) Assesment of the SG lower bound for fixed values of θ_c.

Fig. 4: Analysis of the joint metric. The parameters selected are $h_U = 1.5m$, $h_B = 6m$, $\lambda_S = 5km^{-1}$, $\lambda_B = 5km^{-1}$, $P_B = 1W$, $f = 3.6GHz$, $\alpha_L = 1.7$, $\alpha_N = 2.5$, $\alpha_D = 3.5$, $\kappa_L = \kappa_N = \kappa_D = (4\pi f/c)^2$, $\eta = 0.1$, $\beta = 0.0004$, $\gamma = 1$ and $K = 6$.

in Figure 6b. One can note that even if the BS density is optimized for each pair (P_B, β), the cases of low blockage probability and high transmit power lead to the highest optimal capacity values.

V. RAY TRACING-BASED VALIDATION

A. RT network topology

In the framework of the RT simulations, the studied environments are identical to the SG model, up to the following modifications:

- Streets are given a non-zero width w_S.
- Users and BSs and are located on sidewalks. In a given street, the sidewalk on which each BS is located is randomly chosen. For the sake of practical RT imple-

D. Optimal UE capacity

Figure 6a quantifies the variation of the BS density maximizing the mean capacity as a function of variables β and P_B. This optimal density increases with the blockage probability factor β. Such an increase enables to compensate for the impact of β on the probability of obtaining a NLOS serving BS. Regarding the transmit power, the SNR values are by definition proportional to P_B and therefore decrease when its value is reduced. To compensate for this effect, the optimal BS density therefore increases to lower the path affecting the serving BS. The corresponding maximal capacities are shown
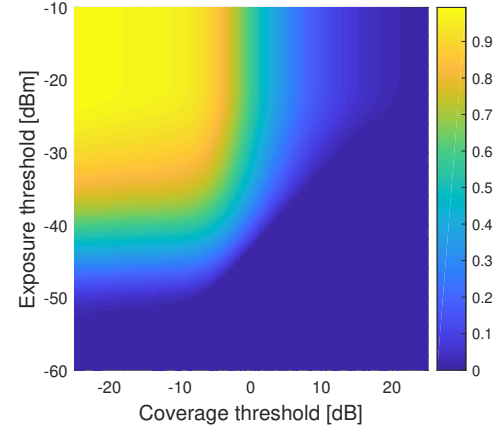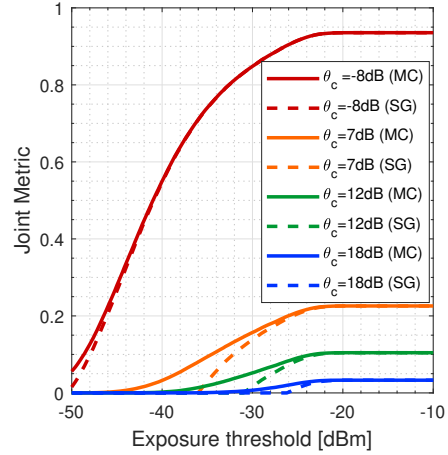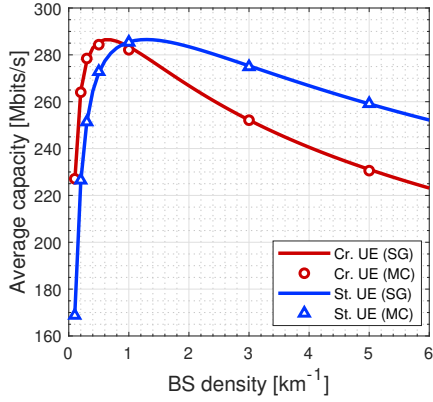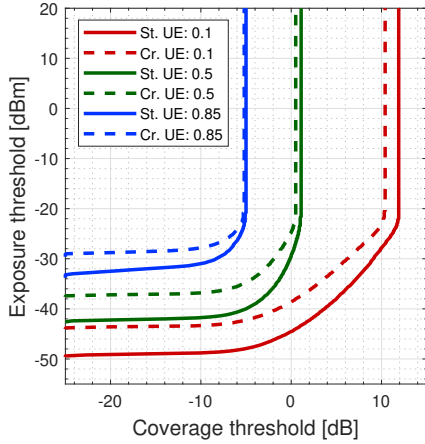
(a) Average UE capacity for $\alpha_L = 2$, $\alpha_N = 2.25$ and $W = -93dBm$.

(b) Isocurves of the joint distribution for $F(\theta_c, \theta_e) \in \{0.1, 0.5, 0.85\}$, $\alpha_L = 2.5$, $\alpha_N = 2.7$ and $W = 0W$.

Fig. 5: Analysis of the differences between street (st.) UE and cross-road (cr.) UE. The selected parameters are $h_U = 1.5m$, $h_B = 4.5m$, $\lambda_S = 5km^{-1}$, $\lambda_B = 5km^{-1}$ (for figure (b)), $f = 3.6GHz$, $\alpha_D = 3.5$, $\kappa_L = \kappa_N = \kappa_D = (4\pi f/c)^2$, $\eta = 0.1$, $\beta = 0.004$, $\gamma = 1$, $B = 100MHz$ and $K = 1$.

mentation, those are placed at a slight distance $d_{B,BU}$ from the buildings walls.

- In order to model obstacles, parallelepipeds (representing cars) are generated with density λ_O in the typical street(s). While the blockage model of the SG framework considers independent blockage probabilities, these obstacles here induce spatial correlations in the blockages experienced by adjacent BSs.

B. RT power computation

The UCLouvain RT software was used in the framework of this study [39]. Two propagation mechanisms are considered by this tool: reflection and diffraction. Also, only outdoor to outdoor scenarios are considered: the potential propagation of
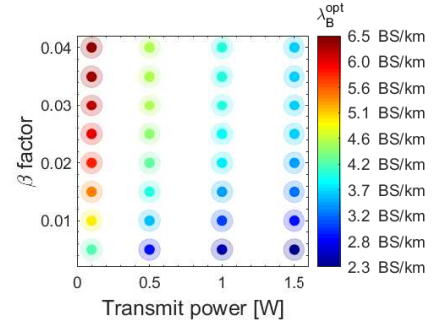
(a) Optimal BS density λ_B^{opt}.
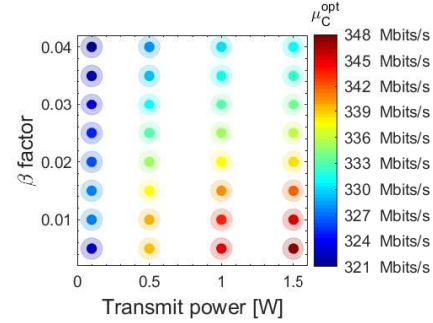
(b) Associated maximal average capacity μ_C^{opt}.

Fig. 6: Analysis of the UE capacity as function of β and P_B. The parameters selected are $h_U = 1.5m$, $h_B = 4.5m$, $\lambda_S = 5km^{-1}$, $\lambda_B = 5km^{-1}$, $f = 3.6GHz$, $\alpha_L = 2.5$, $\alpha_N = 2.75$, $\alpha_D = 3.5$, $\eta = 0.1$, $\beta = 0.004$, $\kappa_L = \kappa_N = \kappa_D = (4\pi f/c)^2$, $\gamma = 1$, $B = 100MHz$, $W = -93dBm$ and $K = 1$.

waves via building penetration is not modelled. To keep the computational time in a reasonable range, at most two interactions are considered between a BS and a UE. In addition, diffraction is only taken into account for the last interaction. These hypotheses seem reasonable as an electromagnetic wave which undergoes more than two interactions or more than one diffraction is strongly attenuated. The computation of the electrical fields for each propagation mechanism is detailed below. One will denote the distance between positions X and Y by d_{XY}.

1) Line of sight: Let $\overline{e}_0$ be the unit vector aligned with the transmitted electric field. The LOS field received from a BS located in B at an observation point P is given by

$$\overline{e}_{LOS}(P) = \overline{e}_0 \frac{e^{-jkd_{BP}}}{d_{BP}}, \qquad (29)$$

where k is the wave number.

2) Reflection: Let Q be a reflection point. Using Fresnel dyadic coefficients $\overline{\overline{R}}$ (computed as in [40]), the reflected field $\overline{e}_{ref}(P)$ at observation point P is given by

$$\overline{e}_{ref}(P) = \overline{\overline{R}} \cdot \overline{e}_{LOS}(Q) \frac{d_{BQ}}{d_{BQ} + d_{QP}} e^{-jkd_{QP}}. \qquad (30)$$

3) Diffraction: Let S be a diffraction point. Using uniform theory of diffraction (UTD), the reflected field $\overline{e}_{diff}(P)$ at

observation point P is given by

$$\overline{e}_{diff}(P) = \overline{\overline{D}} \cdot \overline{e}_{LOS}(S) \sqrt{\frac{d_{BS}}{d_{SP}(d_{BS} + d_{SP})}} e^{-jkd_{SP}},$$

(31)

where $\overline{\overline{D}}$ are the Guevara's coefficients preferred to the usual UTD dyadic coefficients for their reciprocity regarding the ray's incidence [41].

4) Received power: Finally, since $\overline{e}_0$ is normalized at the emission, the received power at a typical user location i^* from a given BS j is given by

$$P_{i^*j}^{(RT)} = P_B \left(\frac{4\pi f}{c}\right)^{-2} ||\overline{e}_{tot} \cdot \overline{e}_{tot}^H|| \tag{32}$$

$$\text{with} \quad \overline{e}_{tot} = \sum_{n=1}^{N_{paths}} \overline{e}_{n,j} \tag{33}$$

where

- N_{paths} is the number of paths coming from this BS and arriving at the typical user under the considered hypotheses.
- P_B is the transmit effective isotropic radiated power.
- c is the speed of light.
- $\overline{e}_{n,j}$ are the electric fields at i^* computed by means of equations (29), (30) and (31).

C. Methodology to fix the parameters

In order to compare the SG and RT approaches, the parameters of the two frameworks should be coherently selected. Table I summarizes these macroparameters.

Parameters common to the RT and SG frameworks
R, h_U, h_B, r_s, λ_S, λ_B, P_B, B and f
Parameters specific to the RT framework
w_S, $d_{B,BU}$ and λ_O.
Ground permittivity: $15 - 1.50j$ (cfr. p. 66-67 of [40])
Building permittivity: $5.3 - 0.42j$ (cfr. p. 66-67 [40])
Parameters specific to the SG framework
β, γ, α_L, α_N, α_D, κ_L, κ_N, κ_D, η, fading models

TABLE I: Parameters employed in the SG and RT frameworks.

In the considered case study, the parameters of the first and second line of table I were set to $R = 2km$, $h_U = 1.5m$, $h_B = 6m$, $r_s = 1m$, $\lambda_S = 5km^{-1}$, $\lambda_B = 5km^{-1}$, $P_B = 1W$, $B = 100MHz$, $f = 3.6GHz$, $w_S = 35m$, $d_{B,BU} = 5m$ and $\lambda_O = 20km^{-1}$. We also set $\kappa_L = \kappa_N = \kappa_D = (4\pi f/c)^2$. From a sufficient amount of RT simulations, we are then able to estimate the other SG parameters based on the statistics of the RT results. The employed methodology consists of the following steps:

- RT simulations are performed for a large number of realizations of the MPLP. At each iteration, the received powers $P_{i^*j}^{(RT)}$ at the typical UE are computed using equation (33). The propagation condition (LOS or NLOS) of each link is also assessed.
- Based on the statistics of these received powers, the parameters β, γ, α_L and α_N are computed using a mean square error method.

- The corresponding fading distribution is then deduced by dividing the received powers by the path losses estimated at the previous step. An analytical fading model is then selected to approximate this empirical distribution.
- The parameter η is independently determined by computing the percentage of users located at crossroads in the RT simulations.

The values obtained for the SG parameters were then $\beta = 0.004$, $\gamma = 0.85$, $\alpha_L = 1.66$, $\alpha_N = 1.93$ and $\eta = 0.02$. The squared fading gains (i.e. fading powers) of the LOS and NLOS links were approximated with exponential distributions of rate parameters 1.66 and 0.33 respectively.
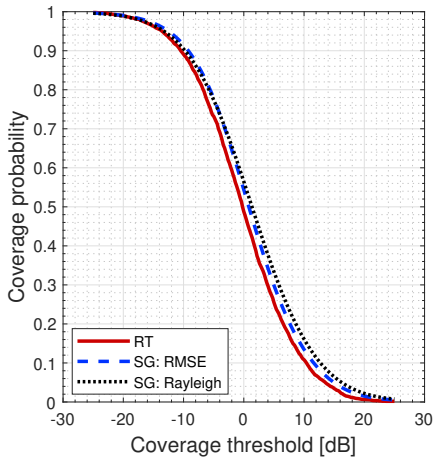
D. Numerical results

Both frameworks were compared for the parameters obtained in the previous section. Figures 7a and 7b illustrate the coverage and exposure distributions. The slight differences between the RT and SG curves can be explained by means of Figure 7c. This figure shows the CDFs of the useful and interfering powers: $P(S > \theta_p)$ and $P(I_L + I_N + I_D > \theta_p)$. One can observe that the contribution of the serving BS in SG is slightly overestimated compared to the RT values. This results in coverage and exposure probabilities which are overestimated as well. Figures 7a and 7b also illustrate the results obtained when SG fading parameters are not optimized with respect to the RT tool. In that case, only the path loss parameters are optimized and the SG fading distribution is taken as normalized Rayleigh (i.e. with squared channel gains modelled via an exponential distribution of unit rate). One will note the loss of accuracy obtained when both path loss and fading aspects are not optimized.
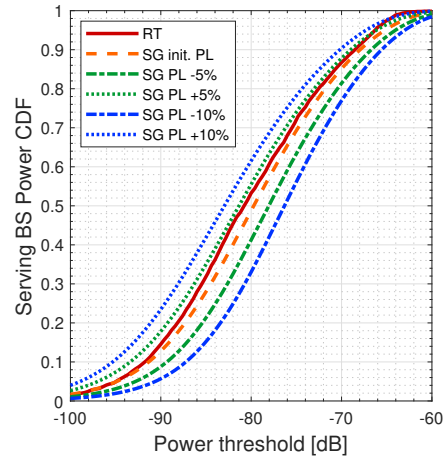
Figure 8 illustrates the sensitivity of the SG model to potential errors in the estimated path loss exponents. Estimation errors of 5 and 10 percents are introduced. The impact on the distributions of the useful power and of the interference is shown in 8a and 8b. One can observe that these errors can lead to significant deviations, which highlights the importance of accurately extracting the parameters if SG is to be used.
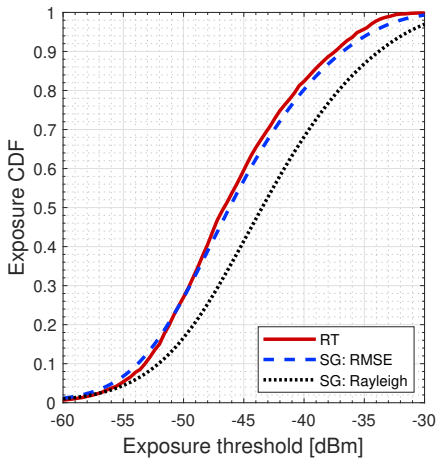
VI. CONCLUSION

In this work, a joint analysis of the data rate and exposure has been conducted for Manhattan environments. This analysis relied on several metrics, computed by means of SG and RT approaches. We have shown that both frameworks could yield similar performance for these metrics. An appropriate estimation of the propagation parameters is however a necessary condition to obtain such a correspondence. The RT validation therefore strengthens the relevance of using SG tools for Manhattan environments. In addition, it reinforces the idea of developing hybrid approaches: the RT tool has the advantage of relying on more physical backgrounds compared to the SG abstraction level. However, it is more time consuming than SG analyses, or than the equivalent MC simulations usually used to validate these SG approaches. When calculating the performance of users in large environments, one might consider combined techniques. On the one hand, power contributions from BSs close to the user could be computed via RT. On the
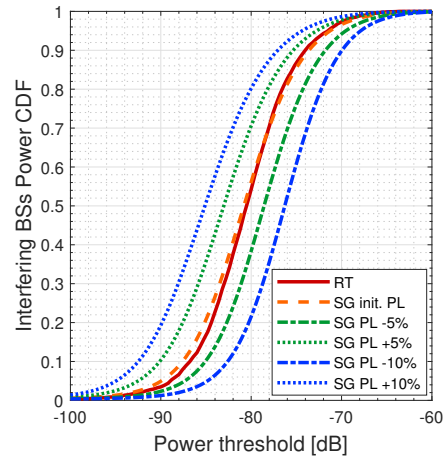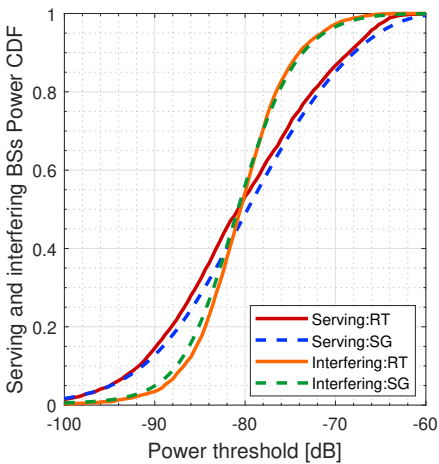
(a) Coverage probability $P_c\left(\theta_c\right)$.

(b) Exposure CDF $P_e\left(\theta_e\right)$.

(c) Received and interfering powers (RMSE only)

Fig. 7: Comparison of SG and RT approaches.

(a) Impact of PL exponents estimation errors on the CDF of the useful received power

(b) Impact of PL estimation errors on the CDF of the aggregate interference

Fig. 8: Sensitivity analysis of the estimated PL exponents based on the CDFs of the useful received power $P\left(S > \theta_p\right)$ and of the aggregate interference $P\left(I_L + I_N + I_D > \theta_p\right)$.

other hand, power contributions from BSs located further away (with less impact) could be computed using these equivalent MC simulations. Such two-fold framework might provide interesting trade-offs in terms of accuracy and computational resources. Several commercial softwares have been built with this line of thought, but with more complex models (see for example [42] combining COST and RT approaches). Our results might hence open the door to further simplifications.

Other work extensions could include the incorporation of beamforming schemes. Moreover, the RT tool could be improved by implementing additional propagation mechanisms (e.g. diffuse scattering). Finally, the analysis might be extended by proposing a comparison to a third framework (e.g. Winner type models).

$$\phi_{L,1}(t|r) = \mathbb{E}_{\Phi_{L,r}}\left[\prod_{j \in \Phi_L(r)} \mathbb{E}_{|h_j|^2}\left[\exp\left(jtP_B|h_j|^2 \kappa_L^{-1}\sqrt{r_j^2 + \Delta H^2}^{-\alpha_L}\right)\right]\right]$$

$$\overset{(1)}{=} \exp\left(-2\lambda_B \int_r^R p_L(r')\left[1 - \mathbb{E}_{|h|^2}\left[\exp\left(jtP_B|h|^2 \kappa_L^{-1}\sqrt{r'^2 + \Delta H^2}^{-\alpha_L}\right)\right]\right]dr'\right)$$

$$\overset{(2)}{=} \exp\left[2\lambda_B \int_r^R p_L(r')\left[\phi_F\left(P_B \kappa_L^{-1}\sqrt{r'^2 + \Delta H^2}^{-\alpha_L}t; K\right) - 1\right]dr'\right]. \tag{34}$$

$$\phi_{D,1}(t|r) = \mathbb{E}_{\Psi_{VS}}\left[\mathbb{E}_{\Psi_{b,k}}\left[\mathbb{E}_{|h_{jk}|^2}\left[\exp\left(\sum_{y_k \in \Phi_{VS}}\sum_{x_{jk} \in \Phi_{b,k}} jtP_B \kappa_D^{-1}|h_{jk}|^2 \mathcal{D}_b(x_{jk},y_k)^{-\alpha_D}\right)\right]\right]\right]$$

$$= \mathbb{E}_{\Phi_{VS}}\left[\prod_{y_k \in \Psi_{VS}} \mathbb{E}_{\Psi_{b,k}}\left[\prod_{x_{jk} \in \Psi_{b,k}} \mathbb{E}_{|h_{jk}|^2}\left[\exp\left(jtP_B \kappa_D^{-1}|h_{jk}|^2 \mathcal{D}_b(x_{jk},y_k)^{-\alpha_D}\right)\right]\right]\right]$$

$$\overset{(1)}{=} \mathbb{E}_{\Phi_{VS}}\left[\prod_{y_k \in \Psi_{VS}} \mathbb{E}_{\Psi_{b,k}}\left[\prod_{x_{jk} \in \Psi_{b,k}} \Phi_F\left(P_B \kappa_D^{-1}\mathcal{D}_b(x,y)^{-\alpha_D}t; 0\right)\right]\right]$$

$$\overset{(2)}{=} \mathbb{E}_{\Phi_{VS}}\left[\prod_{y_k \in \Psi_{VS}} \exp\left(-2\lambda_B \int_{r_s}^R 1 - \Phi_F\left(P_B \kappa_D^{-1}\mathcal{D}_b(x,y)^{-\alpha_D}t; 0\right)dx\right)\right]$$

$$\overset{(3)}{=} \exp\left[-2\lambda_S \int_0^R 1 - \exp\left[-2\lambda_B \int_{r_s}^R 1 - \Phi_F\left(P_B \kappa_D^{-1}\mathcal{D}_b(x,y)^{-\alpha_D}t; 0\right)dx\right]dy\right] \tag{35}$$

$$P_{c,q}^{(p)}(\theta_c|r) \overset{(1)}{=} \mathbb{P}\left[S - \theta_c(I_L + I_N + I_D) > 0\,|\,r\right]$$

$$\overset{(2)}{=} \frac{1}{2} + \frac{1}{\pi}\int_0^\infty Im\left[\phi_S^{(p)}(t|r)\phi_{L,q}(-\theta_c t|r)\phi_{N,q}(-\theta_c t|r)\phi_{D,q}(-\theta_c t)\right]t^{-1}dt. \tag{36}$$

$$P_{c,q}(\theta_c) \overset{(1)}{=} \int_0^R \left(p_L(r)P_{c,q}^{(L)}(\theta_c|r) + p_N(r)P_{c,q}^{(N)}(\theta_c|r)\right)f_{r,q}(r)dt$$

$$\overset{(2)}{=} \frac{1}{2} + \frac{1}{\pi}\int_0^\infty Im\left[\phi_{D,q}(-\theta_c t)\int_{r_0}^R p_L(r)\phi_S^{(L)}(t|r)\phi_{L,q}(-\theta_c t|r)\phi_{N,q}(-\theta_c t|r)f_{r,q}(r)dr\right]t^{-1}dt$$

$$+ \frac{1}{\pi}\int_0^\infty Im\left[\phi_{D,q}(-\theta_c t)\int_{r_0}^R p_N(r)\phi_S^{(N)}(t|r)\phi_{L,q}(-\theta_c t|r)\phi_{N,q}(-\theta_c t|r)f_{r,q}(r)dr\right]t^{-1}dt \tag{37}$$

APPENDIX A
PROOF OF EQUATION (16): CHARACTERISTIC FUNCTION FOR THE LOS INTERFERING LINKS

This proof is inspired by [10]. Let $\Phi_{L,r}$ be the set of interfering BSs located in the typical street in LOS conditions located further than a distance r from the centric user. We denote by $|h_j|^2$, the fading coefficients associated to a BS $j \in \Phi_{L,r}$ and r_j, its distance to the typical user. The characteristic function of the interference coming from $\Phi_{L,r}$ is given by (34) at the top of the page. In the developments of this equation, (1) comes is obtained by definition of the probability generating functional (PGFL) of $\Phi_{L,r}$; (2) comes from the definition of the characteristic function $\Phi_F(\cdot;\cdot)$.

APPENDIX B
PROOF OF EQUATION (18): CHARACTERISTIC FUNCTION OF THE DIFFRACTED LINKS

For this proof, the following notations are introduced:

- Ψ_{VS} it the 1D PPP of the intersections of the vertical streets with the typical UE avenue.
- y_k is the distance between the typical UE and the crossroad with vertical street $k \in \Psi_{VS}$.
- $\Psi_{b,k}$ it the 1D PPP of the BSs in vertical street k.
- x_{jk} is the distance from BS $j \in \Psi_{b,k}$ to the crossroad of street k with the user street.

On the basis of these notations, the CF of the interference associated to diffraction is given by (35). Regarding the successive steps, (1) is obtained by computing the expectation of the fading coefficients, and by definition of $\Phi_F(\cdot,\cdot)$. (2) and (3) come from the definition of the PGFL [37], applied on $\Psi_{b,k}$ then on Ψ_{VS}.

APPENDIX C
PROOF OF EQUATION (20): COVERAGE PROBABILITY OF A TYPICAL UE

Conditioned on the serving distance r and on (p), the propagation condition of the serving BS (LOS or NLOS),

the coverage probability can be expressed as (36) where (1) is obtained by definition of the coverage probability and by rearranging terms and (2) is computed using the Gil-Pelaez theorem [43]. The desired expression is finally given by (37) where (1) is obtained by averaging over the distibution of the serving distance and by using the total law of probability; (2) is obtained by developing the expressions of the conditioned probabilities.

REFERENCES

[1] M. K. Weldon, *The future X network: a Bell Labs perspective.* CRC press, 2016.

[2] K. Ali, "Modeling, analysis, and design of 5g networks using stochastic geometry," Ph.D. dissertation, 2018.

[3] H. Claussen, D. Lopez-Perez, L. Ho, R. Razavi, and S. Kucera, *Small cell networks: deployment, management, and optimization.* John Wiley & Sons, 2017.

[4] A. Osseiran, J. F. Monserrat, and P. Marsch, *5G mobile and wireless communications technology.* Cambridge University Press, 2016.

[5] X. Ge, S. Tu, G. Mao, C.-X. Wang, and T. Han, "5g ultra-dense cellular networks," *IEEE Wireless Communications*, vol. 23, no. 1, pp. 72–79, 2016.

[6] T. K. Geok, F. Hossain, M. Kamaruddin, N. Rahman, S. Thiagarajah, A. T. W. Chiat, and C. Liew, "A comprehensive review of efficient ray-tracing techniques for wireless communication," *International Journal on Communications Antenna and Propagation*, vol. 8, no. 2, pp. 123–136, 2018.

[7] Y. d. J. Bultitude and T. Rautiainen, "Ist-4-027756 winner ii d1. 1.2 v1. 2 winner ii channel models," *EBITG, TUI, UOULU, CU/CRC, NOKIA, Tech. Rep*, 2007.

[8] E. Damosso, L. M. Correia *et al.*, "Cost action 231: Digital mobile radio towards future generation systems: Final report," *European commission*, 1999.

[9] D. He, B. Ai, K. Guan, L. Wang, Z. Zhong, and T. Kürner, "The design and applications of high-performance ray-tracing simulation platform for 5g and beyond wireless communications: A tutorial," *IEEE Communications Surveys & Tutorials*, vol. 21, no. 1, pp. 10–27, 2019.

[10] H. ElSawy, A. Sultan-Salem, M.-S. Alouini, and M. Z. Win, "Modeling and analysis of cellular networks using stochastic geometry: A tutorial," *IEEE Communications Surveys & Tutorials*, vol. 19, no. 1, pp. 167–203, 2016.

[11] F. Baccelli and X. Zhang, "A correlated shadowing model for urban wireless networks," in *2015 IEEE Conference on Computer Communications (INFOCOM).* IEEE, 2015, pp. 801–809.

[12] C.-S. Choi and F. Baccelli, "Poisson cox point processes for vehicular networks," *IEEE Transactions on Vehicular Technology*, vol. 67, no. 10, pp. 10 160–10 165, 2018.

[13] Y. Wang, K. Venugopal, A. F. Molisch, and R. W. Heath, "Mmwave vehicle-to-infrastructure communication: Analysis of urban microcellular networks," *IEEE Transactions on Vehicular Technology*, vol. 67, no. 8, pp. 7086–7100, 2018.

[14] A. I. Akin, I. Stupia, and L. Vandendorpe, "On the effect of blockage objects in dense mimo swipt networks," *IEEE Transactions on Communications*, vol. 67, no. 2, pp. 1059–1069, 2018.

[15] X. Zhang, F. Baccelli, and R. W. Heath, "An indoor correlated shadowing model," in *2015 IEEE Global Communications Conference (GLOBECOM).* IEEE, 2015, pp. 1–7.

[16] M. K. Müller, M. Taranetz, and M. Rupp, "Analyzing wireless indoor communications by blockage models," *IEEE Access*, vol. 5, pp. 2172–2186, 2016.

[17] E. Hriba, M. C. Valenti, and R. W. Heath, "Optimization of a millimeter-wave uav-to-ground network in urban deployments," in *MILCOM 2021-2021 IEEE Military Communications Conference (MILCOM).* IEEE, 2021, pp. 861–867.

[18] B. R. Elbal, M. K. Müller, S. Schwarz, and M. Rupp, "Coverage analysis of relay assisted v2i communication in microcellular urban networks," in *2019 27th European Signal Processing Conference (EUSIPCO).* IEEE, 2019, pp. 1–5.

[19] V. V. Chetlur and H. S. Dhillon, "On the load distribution of vehicular users modeled by a poisson line cox process," *IEEE Wireless Communications Letters*, vol. 9, no. 12, pp. 2121–2125, 2020.

[20] ——, "Coverage analysis of a vehicular network modeled as cox process driven by poisson line process," *IEEE Transactions on Wireless Communications*, vol. 17, no. 7, pp. 4401–4416, 2018.

[21] C.-S. Choi and F. Baccelli, "Modeling and analysis of vehicle safety message broadcast in cellular networks," *IEEE Transactions on Wireless Communications*, vol. 20, no. 7, pp. 4087–4099, 2021.

[22] V. V. Chetlur and H. S. Dhillon, "Coverage and rate analysis of downlink cellular vehicle-to-everything (c-v2x) communication," *IEEE Transactions on Wireless Communications*, vol. 19, no. 3, pp. 1738–1753, 2019.

[23] ——, "Success probability and area spectral efficiency of a vanet modeled as a cox process," *IEEE Wireless Communications Letters*, vol. 7, no. 5, pp. 856–859, 2018.

[24] C.-S. Choi and F. Baccelli, "An analytical framework for coverage in cellular networks leveraging vehicles," *IEEE Transactions on Communications*, vol. 66, no. 10, pp. 4950–4964, 2018.

[25] G. Ghatak, A. De Domenico, and M. Coupechoux, "Small cell deployment along roads: Coverage analysis and slice-aware rat selection," *IEEE Transactions on Communications*, vol. 67, no. 8, pp. 5875–5891, 2019.

[26] W. Lu and M. Di Renzo, "Stochastic geometry modeling of cellular networks: Analysis, simulation and experimental validation," in *Proceedings of the 18th ACM International Conference on Modeling, Analysis and Simulation of Wireless and Mobile Systems*, 2015, pp. 179–188.

[27] S. S. Ram, G. Singh, and G. Ghatak, "Optimization of radar parameters for maximum detection probability under generalized discrete clutter conditions using stochastic geometry," *arXiv preprint arXiv:2101.12429*, 2021.

[28] J.-E. Berg, "A recursive method for street microcell path loss calculations," in *Proceedings of 6th International Symposium on Personal, Indoor and Mobile Radio Communications*, vol. 1. IEEE, 1995, pp. 140–143.

[29] J. Järveläinen, S. L. Nguyen, K. Haneda, R. Naderpour, and U. T. Virk, "Evaluation of millimeter-wave line-of-sight probability with point cloud data," *IEEE Wireless Communications Letters*, vol. 5, no. 3, pp. 228–231, 2016.

[30] S. Singh, M. N. Kulkarni, A. Ghosh, and J. G. Andrews, "Tractable model for rate in self-backhauled millimeter wave cellular networks," *IEEE Journal on Selected Areas in Communications*, vol. 33, no. 10, pp. 2196–2211, 2015.

[31] S. Wang, W. Guo, and M. D. McDonnell, "Distance distributions for real cellular networks," in *Computer Communications Workshops (INFOCOM WKSHPS), 2014 IEEE Conference on.*

IEEE, 2014, pp. 181–182.

[32] L. Raschkowski, P. Kyösti, K. Kusume, and T. Jämsä, "Metis channel model," in *ICT-317669-METIS/D1.4*, 2015.

[33] M. Di Renzo and W. Lu, "System-level analysis and optimization of cellular networks with simultaneous wireless information and power transfer: Stochastic geometry modeling," *IEEE Transactions on Vehicular Technology*, vol. 66, no. 3, pp. 2251–2275, 2017.

[34] F. De Saint Moulin, "Stochastic geometry-based modelling of wireless communication networks : Uav-based networks," Master's thesis, Université Catholique de Louvain, 2020.

[35] M. Fréchet, "Généralisation du théoreme des probabilités totales," *Fundamenta mathematicae*, vol. 1, no. 25, pp. 379–387, 1935.

[36] K. A. Hamdi, "A useful lemma for capacity analysis of fading interference channels," *IEEE Transactions on Communications*, vol. 58, no. 2, pp. 411–416, 2010.

[37] B. François and B. Bartłomiej, *Stochastic geometry and wireless networks: Volume i theory*, 2010.

[38] J. Feng and Z. Feng, "Optimal base station density of dense network: From the viewpoint of interference and load," *Sensors*, 2017.

[39] Q. Gueuning and C. Oestges, "A beam tracer for radio-coverage prediction in urban environnement," *Brussels–Wallonia Auxiliary Radiators for Exposure reduction*, 2015.

[40] C. Oestges, "Propagation modelling of low earth-orbit satellite personal communication systems," PhD dissertation, Université Catholique de Louvain, 2000.

[41] D. Tami, C. G. Rego, D. Guevara, A. Navarro, F. J. Moreira, J. Giménez, and H. G. Triana, "Analysis of heuristic uniform theory of diffraction coefficients for electromagnetic scattering prediction," *International Journal of Antennas and Propagation*, vol. 2018, 2018.

[42] A. communications GmbH, "Wave propagation tool, proman (integrated in aoii), user reference," last accessed 14 June 2022. [Online]. Available: https://www.yumpu.com/en/document/read/7522751/winprop-wave-propagation-tool-proman-awe-communications

[43] J. Gil-Pelaez, "Note on the inversion theorem," *Biometrika*, vol. 38, no. 3-4, pp. 481–482, 1951.